Ce electronic states in $Nd_{0.45-x}Ce_xSr_{0.55}MnO_3$ probed by x-ray absorption spectroscopy and photoemission

T Shirai[1], S Imada[1]‡, A Higashiya[1]§, A Sekiyama[1], S Suga[1], T Muro[2], Y Tanaka[3], K Tamasaku[3], M Yabashi[3], T Ishikawa[3], S Miyasaka[4]‖, Y Tokura[4,5]

[1]Department of Materials Physics, Graduate School of Engineering Science, Osaka University, Toyonaka, Osaka 560-8531, Japan
[2]JASRI, SPring-8, Sayo, Hyogo 679-5198, Japan
[3]RIKEN, SPring-8, Sayo, Hyogo 679-5148, Japan
[4]Department of Applied Physics, Graduate School of Engineering, The University of Tokyo, Bunkyou-ku, Tokyo 113-8656, Japan
[5]RIKEN Center for Emergent Matter Science (CEMS), Wako, Saitama 351-0198, Japan

E-mail: imada@se.ritsumei.ac.jp

Abstract. We have investigated the Ce $4f$ electronic states in Ce doped manganites $Nd_{0.45-x}Ce_xSr_{0.55}MnO_3$ (NCSMO) by means of x-ray absorption spectroscopy(XAS) and hard x-ray photoelectron spectroscopy (HAXPES). The Ce $3d$ XAS shows that the Ce ions exist in the form of the Ce^{3+} and Ce^{4+} mixed-valent states, and we have found that the XAS spectral features change with temperature. The Ce $3d$ XAS and HAXPES spectra for NCSMO agree reasonably well with the calculated results based on the single impurity Amderson model (SIAM), which takes into account the atomic multiplets and two valence bands. The estimated Ce bulk valence of $Nd_{0.15}Ce_{0.3}Sr_{0.55}MnO_3$ decreases from 3.44 to 3.30 with cooling.

PACS numbers: 71.28.+d, 79.60.-i

Submitted to: *J. Phys.: Condens. Matter*

‡ Present address: Department of Physical Sciences, College of Science and Engineering, Ristumeikan University, 1-1-1 Nojihigashi, Kusatsu, Shiga 525-8577, Japan
§ Present address: Institute for Fundamental Sciences, Faculty of Science and Engineering, Setsunan University, Neyagawa, Osaka, 572-8505, Japan
‖ Present address: Department of Physics, Graduate School of Science, Osaka University, Toyonaka, Osaka 560-0043, Japan

It has been revealed that the Ce valence depend strongly on the type of the transition metal in the Ce-doped perovskite transition metal oxides $R_{1-x}Ce_xMO_3$ (R: rare earth or divalent cation; M: transition metal) [1]–[5]. This fact itself is quite natural since two different oxides of Ce, namely CeO_2 and Ce_2O_3 are known. In CeO_2 and Ce_2O_3, the ionic state of Ce is Ce^{4+} with the formal configuration of $[Xe]4f^05d^06s^0$ and Ce^{3+} with $[Xe]4f^15d^06s^0$, respectively. When Ce^{4+} replaces R^{3+} in $R_{1-x}Ce_xMO_3$, the valence M becomes $3-x$. In other words, electrons are doped to the valence band in the vicinity of the Fermi level (E_F). On the other hand, when Ce^{3+} replaces R^{3+}, the valence of M is kept three and no electron doping occurs. Therefore the ionic state of Ce is expected to play an important role in controlling such properties as colossal magnetoresistance (CMR) behavior[6]–[9].

The above-mentioned dependence of the Ce valence on M in $R_{1-x}Ce_xMO_3$ can be summarized as follows. When light transition metals such as vanadium and titanium, which have only few $3d$ electrons, are on the M site of $R_{1-x}Ce_xMO_3$, the Ce ions generally take the Ce^{3+} state. On the contrary, when heavy transition metals are on the M site, the Ce ions usually become Ce^{4+}. Closely related case is the well-known high temperature superconductor $Nd_{2-x}Ce_xCuO_4$ in which is Ce takes the Ce^{4+} state[10]. This tendency can be understood in such a manner that Ce^{3+} (Ce^{4+}) with larger (smaller) ionic radius is more stable because the lattice constant is larger (smaller) when lighter (heavier) M with larger (smaller) ionic radius occupies the M site. In the case of M = Mn, located in the center of Ms, the ionic state of Ce may be expected to vary depending on the specific composition. For example, Ce ions in $Ca_{0.8}Ce_{0.2}MnO_3$ are considered to take the Ce^{4+} state because Ce L_3 ($2p \rightarrow 5d$) photoabsorption spectrum is much closer to CeO_2 than to $CeRh_2Si_2$, in which Ce ions are known to take the Ce^{3+}state[3]. On the other hand, in $La_{0.47}Ce_{0.2}Ca_{0.33}MnO_3$, 60 % of Ce ions are considered to take the Ce^{4+} state and the remaining 40 % the Ce $^{3+}$ state, based on the comparison between its Ce $3d$ XPS and those of CeO_2 and Ce_2O_3[4].

$Nd_{0.45}Sr_{0.55}MnO_3$ (NSMO) undergoes a transition from paramagnetic insulator(PI) to A-type antiferromagnetic metal(AFM) at the temperature (T) of 220 K[6]. Since Sr ions take the Sr^{2+} state, the formal valence of Mn is 3.55 in NSMO. The Ce-doped systems, $Nd_{0.45-x}Ce_xSr_{0.55}MnO_3$ (NCSMO), exhibit a phase diagram shown in Fig.1(a)[11]. As x increases, the PI to AF transition temperature is lowered. At the same time, the T-dependence of resistivity in the AF phase changes from metallic to semiconducting. A new low-T phase (AF2), whose magnetic properties are not fully understood, appears in the range of $x \geq 0.2$. If the Ce ions exist as Ce^{3+} when Ce ions are doped into NSMO, it would make the mean ionic radius of the R site larger. This would lead to a similar behavior as in $Nd_{0.45-x}La_xSr_{0.55}MnO_3$. On the other hand, if the Ce ions exist as Ce^{4+}, it would be the same as electron doping into the Mn site, resembling the behavior in $Nd_{0.45+x}Sr_{0.55-x}MnO_3$. In these systems, ferromagnetic metal phase is inserted between PI and AF phase for $x > 0.15$ in $Nd_{0.45-x}La_xSr_{0.55}MnO_3$ and for $x > 0$ in $Nd_{0.45+x}Sr_{0.55-x}MnO_3$, and a new low-$T$ magnetic phase is not found. Therefore, the present phase diagram suggests that Ce exists neither as pure Ce^{3+} nor

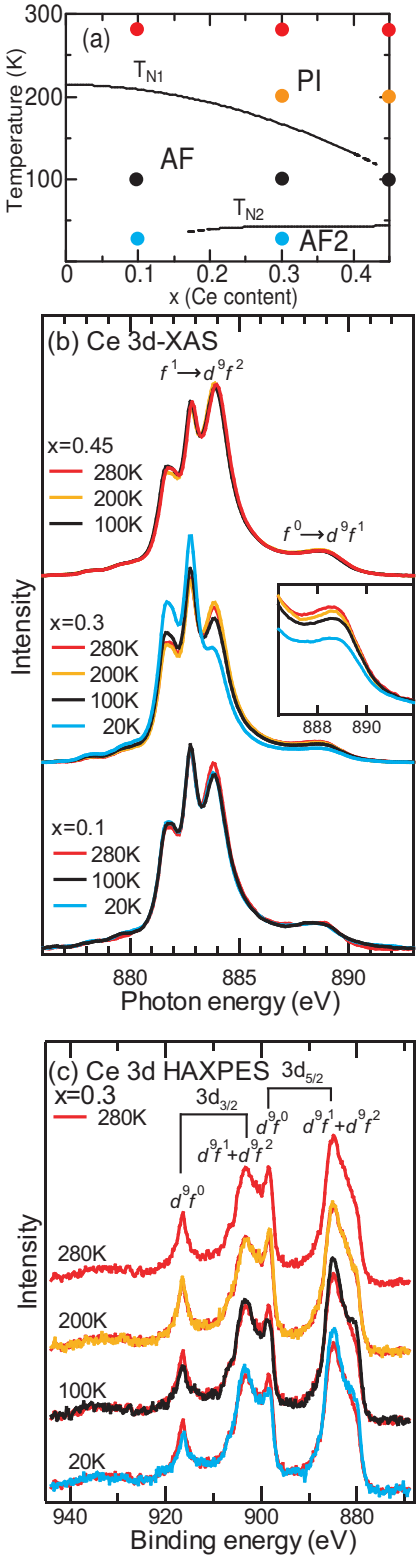

Figure 1. (Colour) (a) The phase diagram of $Nd_{0.45-x}Ce_xSr_{0.55}MnO_3$ (NCSMO).[11] The dots show the measured temperatures (T). (b) The Ce $3d_{5/2}$ XAS spectra of NCSMO(x=0.1, 0.3, 0.45). The inset shows the spectral changes in the vicinity of the f^1 final state of x=0.3. (c) The Ce $3d$ HAXPES spectra of NCSMO(x=0.3).

Table 1. The Ce concentration (x) and temperature (T) dependence of the intensity of the "$f^0 \rightarrow d^9f^1$" component in $Nd_{0.45-x}Ce_xSr_{0.55}MnO_3$ normalized by that of CeO_2. The Ce and Mn valences are roughly estimated based on the calculation shown in Fig. 3. The related discussions are given in the last part of this paper.

x	T(K)	"$f^0 \rightarrow d^9f^1$" intensity	Ce valence	Mn valence
0.45	100-280	0.7	3.53	3.31
0.3	280	0.6	3.44	3.42
	20	0.4	3.30	3.46
0.1	20-280	0.8	3.65	3.49
0				3.55
CeO_2		1	4	

pure Ce^{4+} state. The richness of the phase diagram is expected to come from x and/or T dependence of the Ce electronic state. In order to discuss the mechanism underlying the phase diagram, it is essential to know the Ce electronic state and the Ce valence in NCSMO. In this paper, we report on the Ce 3d x-ray photoabsorption spectroscopy (XAS) studies on $Nd_{0.45-x}Ce_xSr_{0.55}MnO_3$ single crystals with x = 0.1, 0.3 and 0.45, and hard x-ray photoelectron spectroscopy (HAXPES) studies of x = 0.3, for which the clearest T dependence is observed in the Ce 3d XAS. These experimental methods are chosen because they are bulk sensitive. The importance of the bulk sensitivity of the electron spectroscopy has been recognized for rare earth and transition metal compounds [12, 13]. Our discussion will be based on electron spectroscopy experiments on CeO_2[14]–[17] and Ce_2O_3[16] and theoretical analyses of them[18]–[22] by means of the single-impurity Anderson model (SIAM)[23, 24].

Single crystals of $Nd_{0.45-x}Ce_xSr_{0.55}MnO_3$ (x = 0.1, 0.3 and 0.45) were grown by the floating-zone method The clean surfaces of samples were obtained by *in situ* fracturing. The base pressure was better than 4×10^{-8} Pa. The Ce 3d XAS measurements were performed at BL25SU in SPring-8. The XAS spectra were obtained by means of the total electron yield (TEY) method, with the photon energy resolution of $\sim$ 100 meV. The HAXPES measurements were performed at BL19LXU in SPring-8 with use of an MBS A1-HE analyzer. The photon energy $h\nu$ was set to 7934 eV and the Ce 3d core-level photoelectron spectra were measured with the total energy resolution of $\sim$ 500 meV. Probing depth of XAS with TEY method is roughly 10 nm and that of HAXPES with $h\nu$ = 8 keV is roughly 7-8 nm. These probing depths are presently the largest that can be obtained by electron spectroscopy method with good enough energy resolution for above-mentioned purpose.

Figure 1(b) shows the T dependence of the Ce $3d_{5/2}$ XAS spectra of NCSMO (x=0.1, 0.3, 0.45). The spectra are normalized by the integrated intensity in the energy

region displayed here. For all xs and Ts, the Ce $3d$ XAS spectra reveal three remarkable peaks (main peaks) and a satellite which is on the higher photon energy side of the main peaks. The three main peaks are observed at about 881.5, 883 and 884 eV, and the satellite structure is observed at around 889 eV. The satellite has also been observed for CeO_2[17, 20] and other mixed-valent Ce compounds[25]. This structure has been attributed to the $3d^94f^1$ final state, mainly resulting from the $4f^0$ initial state, in other words the Ce^{4+} state. This structure is not seen for Ce_2O_3 in which Ce is in the Ce^{3+} state[16]. Therefore, the intensity of the 889-eV satellite is expected to scale with the ratio between Ce^{4+} and Ce^{3+} initial states. The intensity of this "$f^0 \rightarrow d^9f^1$" structure was estimated by integrating the spectral area after subtracting the background of the "$f^1 \rightarrow d^9f^2$" peak. The results normalized by that for CeO_2 are shown in Table I. Main spectral features observed between 880 and 885 eV have been attributed to the multiplet structures of $3d^94f^2$ final state configurations, mainly resulting from the Ce $3d \rightarrow 4f$ photoexcitation of the Ce^{3+} ($4f^1$) state. However, the $3d^94f^2$ multiplet structures observed for most of the mixed-valent Ce compounds [17, 25] consist of two main peaks, in contrast to the three main peaks in the present case. Both atomic calculation [26] and SIAM calculation for mixed-valent Ce system [20] have yielded a two-component structure due to two groups of multiplet states split by about 2-3 eV. Therefore, the present three-peak line shape suggests an unusual electronic state. This unusual $3d^94f^2$ line-shape will be reproduced by SIAM calculation below.

In the case of $x = 0.45$, nearly no T dependence is seen. This result is consistent with the phase diagram (Fig. 1 (a)). Namely, at 280 K and 200 K the sample is in the PI state, and at 100 K it can be around PI-AF phase transition but the phase transition itself is not clear at this composition. In the case of $x = 0.3$, we have observed drastic T dependence not only in the relative ratio of the three main peaks but also in the intensity of the $4f^0 \rightarrow 3d^94f^1$ satellite as shown in the inset of Fig. 1 (b). Small but finite change is found between 280 K and 200K although both Ts are within the PI phase. Through the PI $\rightarrow$ AF transition, the $4f^0 \rightarrow 3d^94f^1$ satellite decreases and the spectral weight is slightly transferred from the 884 eV peak to the 881.5 eV peak. Through AF $\rightarrow$ AF2 transition, the $4f^0 \rightarrow 3d^94f^1$ satellite decreases further and the 884 eV peak decreases drastically and both the 881.5 and 883 eV peaks increase. The change in the intensity of the $4f^0 \rightarrow 3d^94f^1$ satellite is monotonous through the successive PI $\rightarrow$ AF $\rightarrow$ AF2 transitions. On the other hand, the change in the intensity ratios between the three main peaks is qualitatively different between PI $\rightarrow$ AF and AF $\rightarrow$ AF2 transitions. In the case of x=0.1, a rather small spectral weight transfer from the 884 peak to the 881.5 eV peak is found between 280 K and 100 K. Between 100 K and 20 K, nearly no change was found. This is consistent with the absence of the AF2 phase in this concentration.

Figure 1(c) shows the T dependence of the Ce $3d$ HAXPES spectrum of NCSMO (x=0.3). Shirley type background[27] has been subtracted from each spectrum and the spectra are normalized by the integrated intensity in the energy region displayed here. The spectra of 200 K and below are superimposed on that of 280 K for comparison. We have clearly observed four peak structures at the binding energy (E_B) of about 885,

898.5, 903 and 916.5 eV. These four structures reflect two types of energy splitting. One is the spin-orbit splitting of ∼18 eV between Ce $3d_{5/2}$ and $3d_{3/2}$ core levels (see Fig. 1(c)). The other is the splitting of ∼13.5 eV between the final states with different Ce $4f$ numbers. The structures near 898.5 and 916.5 eV correspond to the $3d^9 4f^0$ final state. On the other hand, the structures near 885 and 903 eV correspond to strongly mixed states consisting of $3d^9 4f^1$ and $3d^9 4f^2$ final state configurations. The spectral shapes have shown noticeable change between 200 and 100 K. The $3d^9 4f^0$ final state is smaller at 100 K than at 200 K. Therefore, it is understood as the weight of the $4f^0$ initial state decreases through the PI→ AF phase transition. As for the $3d^9 4f^1$ and $3d^9 4f^2$ mixed structure around $E_{\rm B} = 885$ eV, the shoulder structure near $E_{\rm B} = 880$ eV becomes slightly larger at 100 K than at 200 K. In the Ce $3d$ HAXPES, essentially no change was found between 100 K (AF phase) and 20 K (AF2 phase). This is in quite a strong contrast to the remarkable difference in Ce $3d$ XAS between the AF and AF2 phases.

For a quantitative analysis of Ce valence, SIAM has widely been applied. Here, we consider a Hamiltonian in the form $H = H_1 + H_2$, where H_1 describes SIAM and H_2 describles the intraatomic interaction related to spin and orbital angular momenta. In SIAM, the atom whose core electron is photoexcited is taken as an impurity atom in the solid, and its localized atomic orbital is assumed to hybridize with the surrounding valence band state. In the present case the Ce atom corresponds to the impurity atom and its $4f$ level hybridizes with the valence band. The Hamiltonian of SIAM is thus written as

$$\begin{aligned} H_1 = & \left[\varepsilon_f - U_{fc}\sum_{\xi}(1-n_{d\xi})\right]\sum_{\nu} n_{f\nu} \\ & + U_{ff}\sum_{\nu>\nu'} n_{f\nu}n_{f\nu'} + \varepsilon_d\sum_{\xi} n_{d\xi} + \sum_i \varepsilon_{ki}\sum_{\nu} n_{i\nu} \\ & + \sum_i V_i \sum_{\nu}\left[\left(\sqrt{\alpha}\right)^{N_f}\left(\sqrt{\beta}\right)^{(10-N_d)} a^+_{i\nu}a_{f\nu} + \text{h.c.}\right]. \end{aligned} \tag{1}$$

The valence band is replaced by levels, and the ith level is assumed to have the energy ε_{ki}. "f" stands for the $4f$ level, and "d" for the $3d$ core-level. ε_f (ε_d) is the energy of the f (d) level. U_{fc} is the attractive Coulomb potential between a core hole and an f electron. U_{ff} is the repulsive Coulomb potential between f electrons. $n_{f\nu}$, $n_{i\nu}$ and $n_{d\xi}$ are the number operators of the f state, the valence band state and the d state, respectively. ν (ξ) is a combined index representing the spin and orbital states of the f (d) symmetry state. V_i is the hybridization between the f level and the ith conduction band level. α and β, representing the dependence of hybridization on the number of f electrons $N_f = \sum_\nu n_{f\nu}$ and that of the d electrons $N_d = \sum_\xi n_{d\xi}$, were set as 2.0 and 0.28, respectively[29]. When Ce $4f$ electron number increases from one to two, the Ce $4f$ orbital expands due to electron-electron repulsion, leading to a larger hybridization. When a core-hole is created, the Ce $4f$ orbital shrinks due to the attractive potential

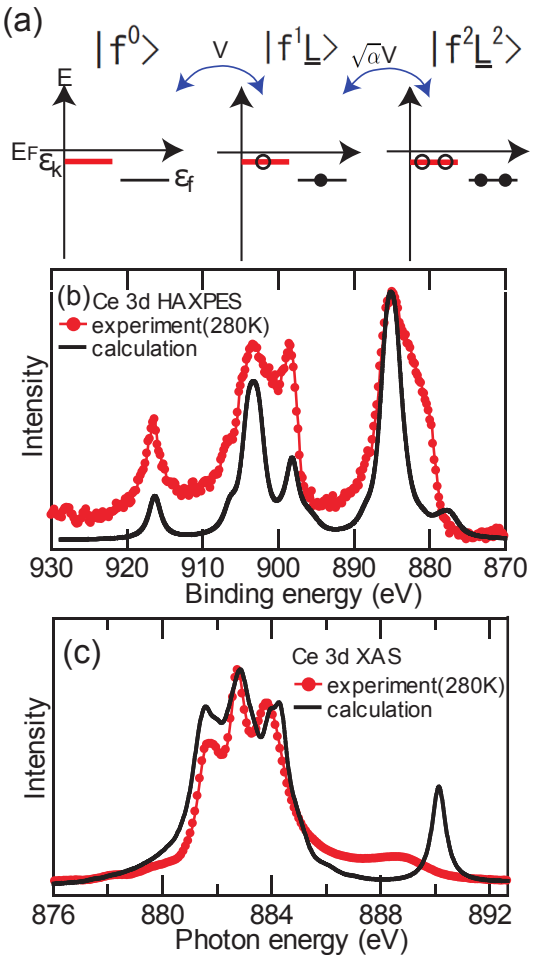

Figure 2. (Colour online) (a)The initial states of the single impurity Amderson model (SIAM) of the one valence band considering the atomic multiplets. (b)The Ce $3d$ HAXPES spectra of NCSMO (x=0.3, 280 K) (red dots). A solid line is SIAM fitting result. (c) The Ce $3d_{5/2}$ XAS spectra of NCSMO (x=0.3, 280 K) (red dots). A solid line is SIAM fitting result.

of the core-hole, leading to a smaller hybridization. H_2 is expressed as

$$H_2 = H_{\rm ee} + H_{\rm so} \tag{2}$$

where $H_{\rm ee}$ is the electron-electron interaction and $H_{\rm so}$ is the spin-orbit interaction of $4f$ and $3d$ electrons[26]. H_2 gives rise to the atomic multiplet structures. The calculations of spectra were performed by with the program developed by Tanaka[28].

At first, we have considered one valence band level, taking into account the initial states shown in Fig.2(a). ϵ_k is the energy of the valence band level. We compare in Fig.2(b) the Ce $3d$ HAXPES spectrum of NCSMO (x=0.3, 280 K) (red dots) and the one valence band SIAM fitting result (solid line), and in Fig.2 (c) the Ce $3d_{5/2}$ XAS spectrum of NCSMO (x=0.3, 280 K) (red dots) and the one valence band SIAM fitting result (solid line). The adopted parameters for fitting the spectra using the one valence band model are listed in Table 2. We have controlled the parameters so that (1) the calculated Ce $3d$ HAXPES roughly reproduces peak position and the intensity of d^9f^0

Table 2. The adopted parameters for fitting the spectra using the one valence band model.

Δ (eV)	V (eV)	U_{ff} (eV)	U_{fc} (eV)
-0.900	0.201	6.55	12.0

peak and (2) the calculated Ce $3d$ XAS roughly reproduces the three-peak structure of the $f^1 \rightarrow d^9f^2$ spectrum. However, the calculated Ce $3d$ HAXPES could not reproduce the structure around 880 eV. In the calculated Ce $3d$ XAS, the $f^0 \rightarrow d^9f^1$ intensity is too large compared to the experiment. The energy difference between the valence band level and the Ce $4f$ state corresponds to the charge transfer energy ($\Delta \equiv \varepsilon_f - \varepsilon_k$). The charge transfer energy Δ is -0.9 eV, which means that the energy of the Ce $4f$ state (ε_f) is lower than that of the valence band level (ε_k). We can interpret that the valence band level represents the part of the valence band in the vicinity of $E_{\rm F}$. However, there is another part of the valence band, namely the O $2p$ band, with which the Ce $4f$ state is expected to hybridize strongly. The O $2p$ band is expected to exist on the lower energy (larger binding energy) side than the Ce $4f$ state. The one valence band model hence cannot reproduce the hybridization between the O $2p$ band and the Ce $4f$ state.

Therefore, we have considered SIAM with two valence band levels illustrated in Fig.3(a). The level at ε_{k1} represents the valence band in the vicinity of $E_{\rm F}$ and that at ε_{k2} represents the O $2p$ band. We compare in the upper part of Fig.3 (b) the Ce $3d$ HAXPES spectrum of NCSMO (x=0.3, 280 K) (red dots) and the two valence band levels SIAM fitting result (solid line), and in top of Fig.3 (c) the Ce $3d_{5/2}$ XAS spectrum of NCSMO (x=0.3, 280 K) (red dots) and the two valence bands SIAM fitting result (solid line). The adopted parameters for fitting the spectra using the two valence bands model are listed in Table 3, where $\Delta_i \equiv \varepsilon_f - \varepsilon_{ki}$. The XAS and HAXPES spectra can be better reproduced by this two valence bands model than by the one valence band model. This reconfirms that both O $2p$ band and the valence band near $E_{\rm F}$ play essential roles in determining the Ce $4f$ electronic state.

We also tried to reproduce the T dependence of NCSMO ($x = 0.3$). The XAS and HAXPES spectra of $T = 280$ K and 20 K can be reproduced by changing the hybridization strength between Ce $4f$ state and the valence band with higher binding energy (V_2), which is shown in bottom of Fig. 3 (b) and Fig. 3 (c), respectively. Red (blue) lines adopt V_2=0.620 (0.616) eV and roughly reproduce the spectra at $T = 280$ K (20 K). Weights of the different configurations in the initial state are listed in Table 4. The small change in V_2 of less than 1 % leads to rather large changes in the weights of different configurations. A rough sketch of how different configurations hybridize with each other to result in the ground states ("g. st.") is shown in Fig. 3 (d). In this diagram, $|f^2\underline{L_1}^2\rangle$ and $|f^2\underline{L_2}^2\rangle$, the weight of which is small, are neglected for simplicity. Since V_2 is much larger than V_1, we first consider the effect of V_2. Namely, we consider the bonding state between $|f^0\rangle$ and $|f^1\underline{L_2}\rangle$ (between $|f^1\underline{L_1}\rangle$ and $|f^2\underline{L_1}\,\underline{L_2}\rangle$) and call it

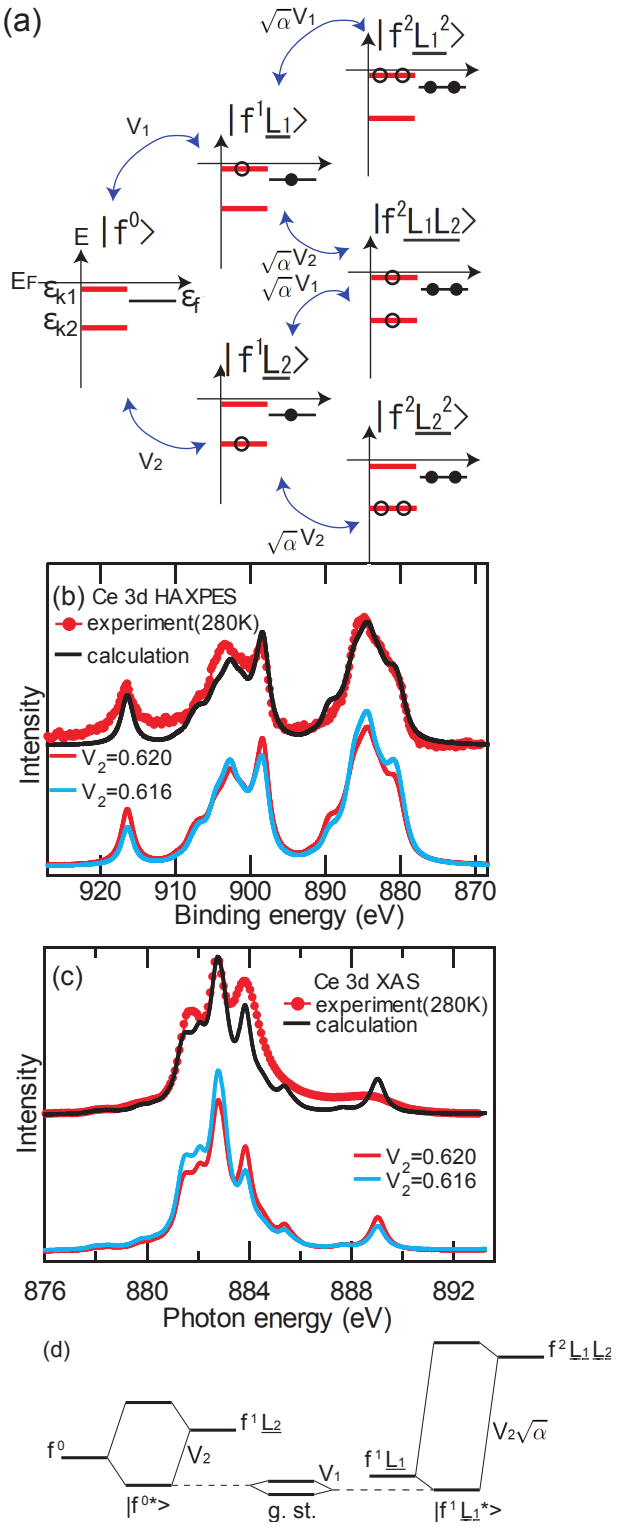

Figure 3. (Colour) (a)The initial states of the single impurity Anderson model (SIAM) of the two valence bands to consider the atomic multiplets. (b)Top: The Ce 3*d* HAXPES spectra of NCSMO (x=0.3, 280 K) (red dots). A solid line is SIAM fitting result. Bottom:V_2 dependence of SIAM result reproducing the T dependence (The red (blue) line is with V_2=0.620 (0.616) eV reproducing the experiment at T = 280 (20) K). The red and blue colors correspond to those in Fig. 2. (c)Top: The Ce $3d_{5/2}$ XAS spectra of NCSMO (x=0.3, 280 K) (red dots). A solid line is SIAM fitting result. Bottom:V_2 dependence of SIAM result reproducing the T dependence. (d) A schematic diagram showing the property of the ground state of the initial state of SIAM.

Table 3. The adopted parameters for fitting the spectra using the two valence bands model.

Δ_1 (eV)	V_1 (eV)	Δ_2 (eV)	V_2 (eV)	U_{ff} (eV)	U_{fc} (eV)
-1.102	0.008	1.70	0.62	8.0	12.0

Table 4. Calculated Ce $4f$ configurations in the initial state and the Ce valence

V_2 (eV)	$\|f^0\rangle$	$\|f^1\underline{L_1}\rangle$	$\|f^1\underline{L_2}\rangle$	$\|f^2\underline{L_1}^2\rangle$	$\|f^2\underline{L_1}\,\underline{L_2}\rangle$	$\|f^2\underline{L_2}^2\rangle$	Ce valence
0.620	22.0 %	51.2 %	19.9 %	0.0 %	4.6 %	2.2 %	3.44
0.616	15.1 %	64.2 %	13.5 %	0.0 %	5.7 %	1.5 %	3.30

$|f^{0*}\rangle$ ($|f^1\underline{L_1}^*\rangle$). The ground state can then be considered as the bonding state between $|f^{0*}\rangle$ and $|f^1\underline{L_1}^*\rangle$ through hybridization V_1.

As illustrated in Fig. 3 (a), the electronic state of the valence band in the vicinity of E_F is the same for $|f^0\rangle$, $|f^1\underline{L_2}\rangle$ and $|f^2\underline{L_2}^2\rangle$. Therefore, not only $|f^0\rangle$ but also $|f^1\underline{L_2}\rangle$ and $|f^2\underline{L_2}^2\rangle$ should be categorized as Ce^{4+} state. In fact, experimental results on CeO_2 have been successfully interpreted by considering electronic states corresponding to $|f^0\rangle$, $|f^1\underline{L_2}\rangle$ and $|f^2\underline{L_2}^2\rangle$ with the weights of 55.4 %, 43.1 % and 1.4 %, respectively[18]. On the other hand, $|f^1\underline{L_1}\rangle$ and $|f^2\underline{L_1}\,\underline{L_2}\rangle$ can be considered as Ce^{3+} state since one hole exists in the valence band in the vicinity of E_F. Finally, $|f^2\underline{L_1}^2\rangle$ corresponds to the Ce^{2+} state. Based on these definitions, Ce valence can be calculated as shown in Table 4. The estimated Ce bulk valence hence decreases from 3.44 to 3.30 with cooling from 280 K to 20 K in $x = 0.3$. If we fit the relation between the Ce valence and the "$f^0 \rightarrow d^9f^1$" intensity in the Ce $3d$ XAS of CeO_2 and NCSMO with $x = 0.3$ at 280 K and 20 K using a third order polynomial, Ce valence of NCSMO with $x = 0.1$ and $x = 0.45$ can be roughly estimated as shown in Table 1. Mn valence estimated using the Ce valence is also shown in Table 1. The decrease of Mn valence with respect to 3.55 of NSMO ($x = 0$), in other words the number of doped electrons per Mn, is not proportional to x and also is T dependent in the case of $x = 0.3$.

Here, we note that $|f^{0*}\rangle$ ($|f^1\underline{L_1}^*\rangle$) state in Fig. 3 (d) corresponds to the Ce^{4+} (Ce^{3+}) state. If V_1 is zero, either of the pure $|f^{0*}\rangle$ or the pure $|f^1\underline{L_1}^*\rangle$, that has the lower energy, becomes the ground state and the Ce valence becomes either 4 or 3, respectively. The small but finite V_1 is the origin of the intermediate Ce valence. Since the nearest neighbors of the Ce site are oxygen atoms, the origin of the ε_{k1} band is most likely the small but finite O $2p$ partial density of states in the vicinity of E_F. This state is expected to hybridize strongly with the Mn $3d$ state. Through this channel and the channel of electron doping mentioned in the last paragraph, the Ce $4f$ electronic states have strong influences on the Mn $3d$ electronic states, giving rise to the rich magnetic and transport properties of NCSMO.

In conclusion, Ce $3d$ XAS shows that the Ce ions exist in the Ce^{3+} and Ce^{4+} mixed-valent states in $Nd_{0.45-x}Ce_xSr_{0.55}MnO_3$, and we find that the XAS spectral feature of

$x = 0.3$ depend strongly on T. The measured Ce $3d$ XAS and HAXPES spectra for NCSMO agree reasonably well with the calculation using the single impurity Anderson model (SIAM) considering the atomic multiplets and the two valence band levels. These two valence band levels represent the valence band in the vicinity of $E_{\rm F}$ and the O $2p$ band. The Ce valence has been found to depend on both x and T. This indicates that the change in the Ce valence plays an essential role in the phase transitions of NCSMO.

The Ce $3d$ XAS measurement at BL25SU of SPring-8 was performed under proposal No. 2000B0338-NS-np. This work was in part supported by Funding Program for World-Leading Innovative R & D on Science and Technology (FIRST Program).

References

[1] Katsufuji T and Tokura Y, 2000 *Phys. Rev.* **62** B 10797
[2] Reehuis M, Ulrich C, Pattison P, Miyasaka M, Tokura Y and Keimer B 2008 *Eur. Phys. J.* **64** B 27
[3] Zeng Z, Greenblatt M and Croft M 2001 *Phys. Rev.* **63** B 224410
[4] Alejandro G, Lamas D G, Steren L B, Gayone J E, Zampieri G, Caneiro A, Causa M T and Tovar M 2003 *Phys. Rev.* **67** B 064424
[5] Balamurugan S, Yamaura K, Arai M and Takayama-Muromachi E 2007 *Phys. Rev.* **76** B 014414
[6] Kuwahara H, Okuda T, Tomioka Y, Asamitsu A and Tokura Y 1999 *Phys. Rev. Lett.* **82** 4316
[7] von Helmolt R, Wecker J, Holzapfel B, Schultz L and Samwer K 1993 *Phys. Rev. Lett.* **71** 2331
[8] Tokura Y, Urushibara A, Moritomo Y, Arima T, Asamitsu A, Kido G and Furukawa N 1994 *J. Phys. Soc. Japan* **63** 3931
[9] Urushibara A, Moritomo Y, Arima T, Asamitsu A, Kido G and Tokura Y 1995 *Phys. Rev.* **51** B 14103
[10] Suzuki T, Nagoshi M, Fukuda Y, Oh-ishi K, Syono Y and Tachiki M 1990 *Phys. Rev.* **42** B 4263
[11] Miyasaka S and Tokura Y unpublished
[12] Sekiyama A, Iwasaki T, Matsuda K, Saitoh Y, Onuki Y and Suga S 2000 *Nature* **403** 396
[13] Suga S *et al* 2005 *J. Phys. Soc. Japan* **74** 2880.
[14] Burroughs P, Hamnett A, Orchard A F and Thornton G 1976 *J. Chem. Soc., Dalton Trans.* **1976**, 1686
[15] Wuilloud E, Delley B, Schneider W-D and Baer Y 1984 *Phys. Rev. Lett.* **53** 202
[16] Allen J W 1985 *J. Magn. Magn. Mater.* **47-48** 168
[17] Kaindl G, Kalkowski G, Brewer W D, Sampathkumaran E V, Holtzberg F, Schach v. Wittenau A 1985 *J. Magn. Magn. Mater.* **47-48** 181
[18] Kotani A, Mizuta H, Jo T and Parlebas J C 1985 *Solid State Commun.* **53** 805
[19] Jo T and Kotani A 1986 *J. Phys. Soc. Japan* **55** 2457
[20] Jo T and Kotani A 1988 *Phys. Rev.* **38** B 830
[21] Imada S and Jo T 1989 *J. Phys. Soc. Japan* **58** 2665
[22] Imada S and Jo T 1990 *Phys. Scr.* **41** 115
[23] Kotani A and Toyozawa Y 1974 *J. Phys. Soc. Japan* **37** 912
[24] Gunnarsson O and Schönhammer K 1983 *Phys. Rev.* **28** B 4315
[25] Jung R-J, Choi B-H, Oh S-J, Kim H-D, Cho E-J, Iwasaki T, Sekiyama A, Imada S, Suga S and Park J G 2003 *Phys. Rev. Lett.* **91** 157601
[26] Thole B T, van der Laan G, Fuggle J C, Sawatzky G A, Karnatak R C and Esteva J-M 1985 *Phys. Rev.* **32** B 5107
[27] Shirley D A 1972 *Phys. Rev.* **5** B 4709
[28] Tanaka A, Jo T and Sawatzky G A,1992 *J. Phys. Soc. Japan* **61** 2636
[29] Gunnarsson O and Jepsen O 1988 *Phys. Rev.* **38** B 3568